Self-Organization, Computational Maps, and Motor Control
P. Morasso and V. Sanguineti (Editors)

HUMAN ARM IMPEDANCE IN MULTI-JOINT MOVEMENTS

Toshio Tsuji
Computer Science and Systems Engineering
Hiroshima University
Kagamiyama 1-chome, Higashi-Hiroshima, 739 (JAPAN)
e-mail : tsuji@huis.hiroshima-u.ac.jp

Abstract

While a subject maintains a given hand location with a specified muscle activation level or a hand force, small external disturbances are applied to his hand by a manipulandum. The corresponding force and displacement vectors are measured in order to estimate the hand impedance by means of a second-order linear model. In this chapter, the spatial features of the estimated hand impedance are discussed with consideration of effects of arm posture and muscle activity.

1 Introduction

Understanding the impedance characteristics of the human arm has lately attracted considerable attention. Several studies have been made for single-joint arm movements. Especially in terms of impedance characteristics of the elbow joint, it has been shown that viscoelastic coefficients change depending on the activation level of muscles (Cannon & Zahalak 1982), task instruction to the subjects (Lacquaniti et al. 1982), joint angles (MacKay et al. 1986), presence and absence of dynamic arm movements (Bennett et al. 1992), and speed of the arm movement and loading (Milner 1993). Unfortunately, impedance properties of multi-joint arm movements cannot be predicted from experimental results

with single-joint arm movements because of viscoelastic properties of the shoulder joint and interactions between joints caused by multi-joint muscles.

For the multi-joint arm movements, Mussa-Ivaldi et al. (1985) developed an experimental method to measure human hand stiffness while maintaining posture. The hand of the subject was displaced from an equilibrium position by a two-joint manipulandum and then the restoring forces were measured at steady-state (from 0.6 s to 1.1 s after the onset of the external disturbance). The hand stiffness characteristics computed from the displacements and forces indicated that the hand stiffness systematically depended on the hand locations and arm postures in the horizontal plane, and that the subjects could not regulate the orientations and shapes of the stiffness ellipses. Flash & Mussa-Ivaldi (1990) showed that the spatial variations of the hand stiffness ellipses in the horizontal plane could be explained by a covariation between the shoulder stiffness and the stiffness component provided by two-joint muscles. Then, Dolan et al. (1993) extended the experimental method developed by Mussa-Ivaldi et al. (1985) to include measurement of dynamic components such as viscosity and inertia as well as stiffness. They showed that the viscosity ellipses tended to have the similar orientation as the corresponding stiffness ellipses. Their estimated results of the hand inertia, however, considerably differed from the calculated values using a two-joint mechanical model of the human subject and varied depending on the filtering method applied to the measured signals. Also, no appropriate explanation has been made yet for the reason why those spatial features of human hand impedance were observed.

On the other hand, it is well known that the viscoelastic property of skeletal muscles, which is a major source of human hand viscoelasticity, largely changes depending on their activation levels (Dowben 1980). Tsuji et al. (1994) pointed out that muscle contraction for a grip force increases the hand stiffness and viscosity, because greater voluntary muscle activation is responsible for higher muscle viscoelasticity. Also, Gomi et al. (1992) and Gomi & Kawato (1996) estimated hand stiffness during two joint arm movements and argued that dynamic stiffness dif-

fers from the static one because of the neuromuscular activity during movements. Although importance of variable structure of impedance characteristics regulated by a motor command from the central nervous system (CNS) has been pointed out as mentioned above, the previous investigators did not analyze a variation of the hand impedance characteristics under different muscle activation levels.

The characteristics of the hand viscoelasticity must be affected by kinematic property of the human arm, motor control signals from the CNS, individual properties of each muscle, and proprioceptive feedback via the muscle spindle and Golgi tendon organ. For hand stiffness, Flash & Mussa-Ivaldi (1990) examined to what extent the kinematic property of the human arm can explain its spatial variations, and showed that the anatomical factors are not sufficient to account for the observations. They also reported that any uniform and consistent relationship between the EMG signals and joint stiffness could not be found.

The present chapter analyzes the spatial characteristics of the human hand impedance with consideration of effects of arm posture and muscle activity. In order to examine these effects experimentally, three different experimental conditions are chosen: 1) maintaining the arm posture with different hand locations under a constant muscle activation (Tsuji et al. 1994, Tsuji et al. 1995), 2) maintaining the muscle activity in different levels under a specific arm posture, 3) maintaining the hand force in different values and directions under a specific arm posture (Tsuji & Kaneko 1996).

2 Impedance in multi-joint arm

Let us consider a multi-joint arm having m joints. Let the position vectors in the joint coordinates and the end-point coordinates be denoted as $\theta \in \Re^m$ and $X \in \Re^l$, respectively, where l is the number of dimensions of the end-point space. For a human arm, m is larger than l, that is, the arm has redundant joint degrees of freedom. The transformation

from θ to X is given by the following nonlinear equation:

$$X = p(\theta). \tag{1}$$

The Jacobian matrix $J(\theta) = \partial p / \partial \theta \in \Re^{l \times m}$ is a locally linearized transformation matrix, which leads the following relationship:

$$dX = J(\theta) d\theta. \tag{2}$$

Based on the principle of the virtual work between velocity and force in the mechanics (Asada & Slotine 1986), we can have

$$\tau = J^T F, \tag{3}$$

where $\tau \in \Re^m$ and $F \in \Re^l$ are the generalized force vectors in the joint coordinates and the end-point coordinates, respectively.

On the other hand, arm movements are generated by m muscles acting on each joint. Let the muscle length vector and the muscle force vector be denoted as $L \in \Re^n$, which is defined that the extending direction is positive, and $f \in \Re^n$, which is defined that the contracting direction is positive, respectively. The muscle length vector L is determined by a nonlinear function of the joint angle vector θ,

$$L = q(\theta). \tag{4}$$

Locally linearizing (4) around a posture θ, we can see

$$dL = G(\theta) d\theta. \tag{5}$$

The transformation $G(\theta) = \partial q / \partial \theta \in \Re^{n \times m}$ is also the Jacobian matrix that determines the relationship between the joint and muscle movements (Mussa-Ivaldi 1986). In a similar manner to (3), the transformation from f to τ is given by

$$\tau = -G^T f. \tag{6}$$

The impedance, which is a general term for stiffness, viscosity and inertia, provides the static and dynamic relations between force and

motion (Hogan 1985). First, let us consider the stiffness relationships among the muscle, joint and end-point levels. The three kinds of stiffness matrices are defined as follows:

$$\text{1) end-point level:} \quad F = -K_e dX \tag{7}$$

$$\text{2) joint level :} \quad \tau = -K_j d\theta \tag{8}$$

$$\text{3) muscle level :} \quad f = K_m dL \tag{9}$$

where $dX = X - X^e$, $d\theta = \theta - \theta^e$ and $dL = L - L^e$. X^e, θ^e and L^e denote equilibrium points of the corresponding vectors and $K_e \in \Re^{l \times l}$, $K_j \in \Re^{m \times m}$, $K_m \in \Re^{n \times n}$ are the stiffness matrices in the end-point, joint and muscle levels, respectively. The muscle stiffness matrix K_m is adjustable through the variable viscoelastic properties of the skeletal muscles and the proprioceptive reflexes (Dowben 1980).

The stiffness relationships among three levels can be derived using (2) - (5) as follows:

$$K_j = J^T K_e J \tag{10}$$

$$= G^T K_m G. \tag{11}$$

Also, the transformations of the viscosity matrices, which are the relationships between force and velocity, are given by

$$B_j = J^T B_e J \tag{12}$$

$$= G^T B_m G, \tag{13}$$

where $B_e \in \Re^{l \times l}$, $B_j \in \Re^{m \times m}$, $B_m \in \Re^{n \times n}$ are the viscosity matrices in the end-point, joint and muscle levels, respectively. Figure 1 shows the transformation between the force and motion by the stiffness and viscosity matrices.

Next, the transformation of the inertia matrix is considered. In general, a motion equation of a multi-joint arm can be written as

$$M(\theta)\ddot{\theta} + h(\theta, \dot{\theta}) + g(\theta) = \tau, \tag{14}$$

where $M(\theta)$ is the non-singular inertia matrix, $h(\theta, \dot{\theta})$ is the Coriolis and centrifugal term, and $g(\theta)$ is the gravity term. Using the relationships between the joint acceleration and the end-point one given

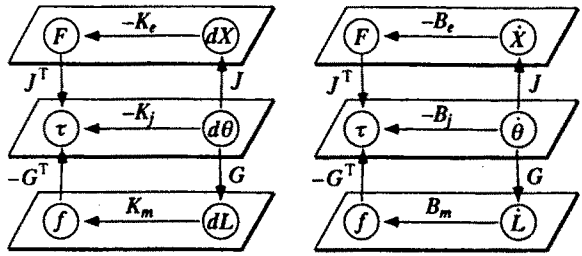

Figure 1: Impedance relationships among muscle, joint and end-point levels. (a) Transformations of stiffness matrices and (b) transformations of viscosity matrices

by

$$\ddot{X} = J\ddot{\theta} + \dot{J}\dot{\theta}, \tag{15}$$

we have (Khatib 1987)

$$\Lambda_e(\theta)\ddot{X} + h_e(\theta,\dot{\theta}) + g_e(\theta) = F, \tag{16}$$

where

$$\Lambda_e(\theta) = (JM^{-1}J^T)^{-1}, \tag{17}$$

$$h_e(\theta,\dot{\theta}) = \bar{J}^T h(\theta,\dot{\theta}) - \Lambda_e(\theta)\dot{J}\dot{\theta}, \tag{18}$$

$$g_e(\theta) = \bar{J}^T g(\theta), \tag{19}$$

and

$$\bar{J} = M^{-1}J^T\Lambda_e(\theta). \tag{20}$$

$\bar{J} \in \Re^{m\times l}$ is a generalized inverse of the Jacobian matrix and $\Lambda_e \in \Re^{l\times l}$ is the inertia matrix represented in the end-point level.

Consequently, the relationships among the muscle, joint and end-point movements can be represented by two kinds.of the Jacobian matrices, J and G.

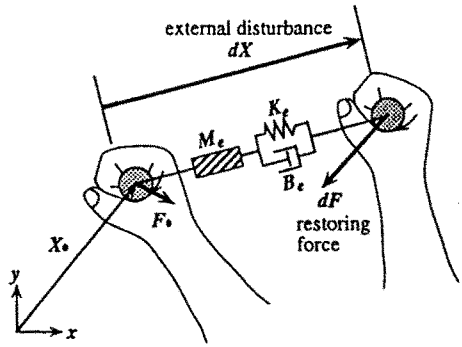

Figure 2: Description of hand impedance for small motions around an equilibrium posture

3 Estimation of human hand impedance

3.1 Impedance model

The following hand impedance model is assumed in the end-point level:

$$M_e(t)\ddot{X}(t) + B_e(t)\dot{X}(t) + K_e(t)(X(t) - X_v(t)) = -F(t), \qquad (21)$$

where $X(t) \in \Re^l$ is the hand position vector; $F(t) \in \Re^l$ is the force vector exerted by the hand to the environment; $X_v(t) \in \Re^l$ represents a virtual equilibrium point (or a virtual trajectory); and $M_e(t), B_e(t)$ and $K_e(t) \in \Re^{l \times l}$ represent hand inertia, viscosity and stiffness matrices, respectively. $M_e(t)$ is the equivalent inertia evaluated in the task space, which may be strongly dependent upon arm postures. The hand viscosity $B_e(t)$ and hand stiffness $K_e(t)$ also depend on the viscoelastic properties of skeletal muscles, low-level neural reflexes and passive elements such as skins and veins.

In order to estimate the hand impedance, the hand of the subject is displaced from an equilibrium by means of a small disturbance of short duration (Fig.2). This kind of the disturbance is necessary in order to assume the approximate constancy of $M_e(t), B_e(t)$ and $K_e(t)$, which are known to depend on posture in a smooth way. As a result, hand inertia, viscosity and stiffness are assumed to be constant after

the onset of the disturbance. Then we can limit ourselves to a constant parameter, second order, linear impedance model of the hand dynamics for small motions:

$$M_e\ddot{X}(t) + B_e\dot{X}(t) + K_e(X(t)\ X_v(t)) = -F(t). \tag{22}$$

Also, since at the onset time t_0 of the disturbance we have

$$M_e\ddot{X}(t_0) + B_e\dot{X}(t_0) + K_e(X(t_0) - X_v(t_0)) = -F(t_0), \tag{23}$$

we can get

$$M_e d\ddot{X}(t) + B_e d\dot{X}(t) + K_e dX(t) - K_e(X_v(t) - X_v(t_0)) = -dF(t), \tag{24}$$

where $dX(t) \equiv X(t) - X(t_0)$ and $dF(t) \equiv F(t) - F(t_0)$.

In the present chapter, the virtual trajectory $X_v(t)$ is assumed not to change in a complex way after the onset of the disturbance, since the disturbance is applied in short duration (Tsuji & Kaneko 1996). Then, when the virtual trajectory is assumed to change with a constant velocity as the first-order approximation, we can have

$$X_v(t) = (t - t_0)c + X_v(t_0), \tag{25}$$

where $c \in \Re^l$ is a constant velocity vector of the virtual trajectory. Substituting (25) into (24) yields

$$M_e d\ddot{X}(t) + B_e d\dot{X}(t) + K_e dX(t) - (t - t_0)K_e c = -dF(t). \tag{26}$$

If the specific external disturbance pattern with $dX(t_f) = d\dot{X}(t_f) = d\ddot{X}(t_f) = 0$ that returns to the initial hand position at time t_f is chosen, we can derive

$$K_e c = \frac{dF(t_f)}{t_f - t_0}. \tag{27}$$

Consequently, the following hand impedance model can be obtained:

$$M_e d\ddot{X}(t) + B_e d\dot{X}(t) + K_e dX(t) = -dF_d(t), \tag{28}$$

where

$$dF_d(t) = dF(t) - \frac{t - t_0}{t_f - t_0} dF(t_f). \tag{29}$$

The above equation means that the difference between the hand forces at t_0 and t_f reduces to a change of the virtual trajectory. Then, the hand impedance matrices M_e, B_e, K_e are estimated using (28).

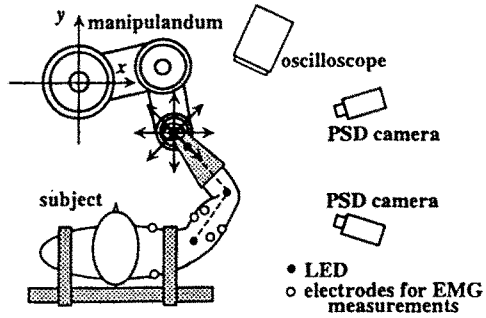

Figure 3: Subject and manipulandum

3.2 Experiments

Figure 3 shows experimental apparatus for hand impedance estimation (Tsuji et al. 1995). A two-joint planar direct drive robot was used as a manipulandum to apply the external displacements to the hand of the subject. The force vector between the hand and the handle was measured by a force sensor attached to the robot handle (resolution 0.05 N for both x- and y- axes). The arm posture of the subject was measured by a stereo-PSD camera system that was able to compute a 3D arm posture from the detected positions of four LED targets attached to the shoulder, elbow and wrist joints of the subject and the robot handle.

The subject took a seat in front of the robot (Fig. 3), similarly to the experimental method developed by Mussa-Ivaldi et al. (1985). The shoulder of the subject was restrained by a belt to the chair back, and the elbow of the right arm was supported in the horizontal plane by a chain attached to the ceiling. The wrist and the hand were fixed by a molded plastic cast (mass 0.164 kg) tightly attached to the robot handle in order to eliminate the need for a voluntary grasping action.

During experiments, surface EMG signals were measured from m. pectoralis major (a single-joint flexor acting on the shoulder joint, which is represented as muscle 1 in Fig. 4), m. infraspinatus (a single-joint extensor acting on the shoulder joint, which is represented as muscle 2 in Fig. 4), m. brachialis (a single-joint flexor acting on the

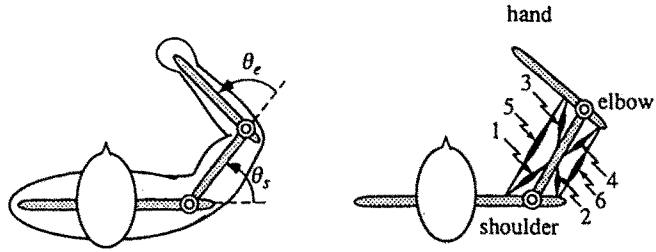

Figure 4: Upper limb model

elbow joint, which is represented as muscle 3 in Fig. 4), m. triceps brachii caput laterale (a single-joint extensor acting on the elbow joint, which is represented as muscle 4 in Fig. 4), m. biceps brachii caput longum (a two-joint flexor, which is represented as muscle 5 in Fig. 4) and m. triceps brachii caput longum (a two-joint extensor, which is represented as muscle 6 in Fig. 4) in order to estimate activation levels of the muscles. After rectification and smoothing by the second order Butterworth filter (cut-off frequency 1 Hz), the EMG signal measured from each muscle was normalized for a value in the maximum voluntary contraction (MVC) of the muscle, which was defined as a muscle activation level α_i $(0.0 \leq \alpha_i \leq 1.0,\ i = 1, \cdots, 6)$.

Under the experimental setup mentioned above, three different sets of the experiments were carried out.

1) *Maintaining posture*

The subject was asked to relax his arm in order to start with a low value of the initial hand force to the handle, and to keep his hand at the initial position. The number of the hand locations used in the experiments was twenty for one subject and eleven for others.

2) *Maintaining muscle activation level*

During experiments, a mean value of the measured activation levels of the flexor and extensor of the two-joint muscles, which correspond to m. biceps brachii caput longum and m. triceps brachii caput longum, respectively, was displayed on the oscilloscope. The subject was asked to maintain the initial hand position while keeping the mean value of the muscle activation levels to a target value. The target muscle acti-

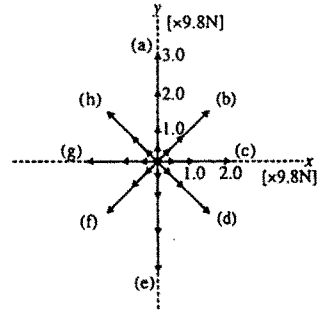

Figure 5: Direction and Amplitude of the target hand forces

vation level was set to seven different values $(0, 5, 10, \cdots, 30$ percents of the MVC).

3) *Maintaining hand force*

The force vector $F(t)$ exerted by the subject's hand to the handle was displayed on the oscilloscope, and the subject was asked to keep the hand force to the instructed direction and amplitude. The target hand force was set to 0.5, 1.0 and 2.0 (×9.8 N) along eight directions shown in Fig. 5. Also, the additional amplitude 3.0 (×9.8 N) was used along y-axis.

In experiment 2), both the flexor and extensor are activated simultaneously, while one of them is mainly activated in experiment 3). It should be noted that the posture ($\theta_s = 1.04$ rad, $\theta_e = 1.57$ rad) shown in Fig. 4 was used as the nominal one in experiments 2) and 3). Also, the muscle activation level and the hand force vector were not presented to the subjects after the onset of the disturbance in order to avoid any effects of the visual feedback.

In all experiments, the external disturbance was applied to his hand by the manipulandum. In order to eliminate any significant influence of voluntary responses of the subject on the measurements, the amplitude of the disturbance which returned to the initial position in a short period was set to 5 mm. The onset time of the disturbance and its direction among eight possible ones (see Fig. 3) were chosen in a random way. Then the hand displacements, $dX(t)$, and hand force, $dF(t)$, were

measured, and the hand velocity, $d\dot{X}(t)$, and acceleration, $d\ddot{X}(t)$, were derived by using a numerical differentiation. The hand impedance, M_e, B_e, K_e, were estimated from (28) by means of the standard least square procedure. The data sampling intervals were 1 ms for the hand forces, positions and the EMG signals, and 10 ms for the 3D arm postures.

Five sets of the experiments for each experimental conditions explained above, where each set includes data corresponding to eight different disturbances, were performed in one day to avoid fatigue of the subject. And this session of the experiments were repeated three days for experiment 1), and six days for experiments 2) and 3) for each subject.

4 Estimated human hand impedance

4.1 Experimental results

Four male subjects, 21–23 years old, performed the required tasks described in the previous section. Figure 6 shows an example of the measured hand displacement $dX(t)$, velocity $d\dot{X}(t)$, acceleration $d\ddot{X}(t)$, and force $dF_d(t)$ in experiment 2), where the target muscle activation level is 10 percent of the MVC. The measured time history of the displacement $dF_d(t)$ (solid lines) well agrees with the predicted value (dashed lines) which is computed by (28) with the estimated hand impedance. The multiple correlation coefficient between the measured and predicted values in Fig. 6 is 0.979. This means that, under our experimental conditions, the hand dynamics of the subject is well approximated by the second-order linear impedance model of (28).

The estimated hand impedance matrices, M_e, B_e and K_e, for all subjects were approximately symmetrical. The symmetrical components of the estimated impedance matrices are used in the following discussions by extracting the corresponding eigenvectors and eigenvalues and displaying them with an elliptical plot.

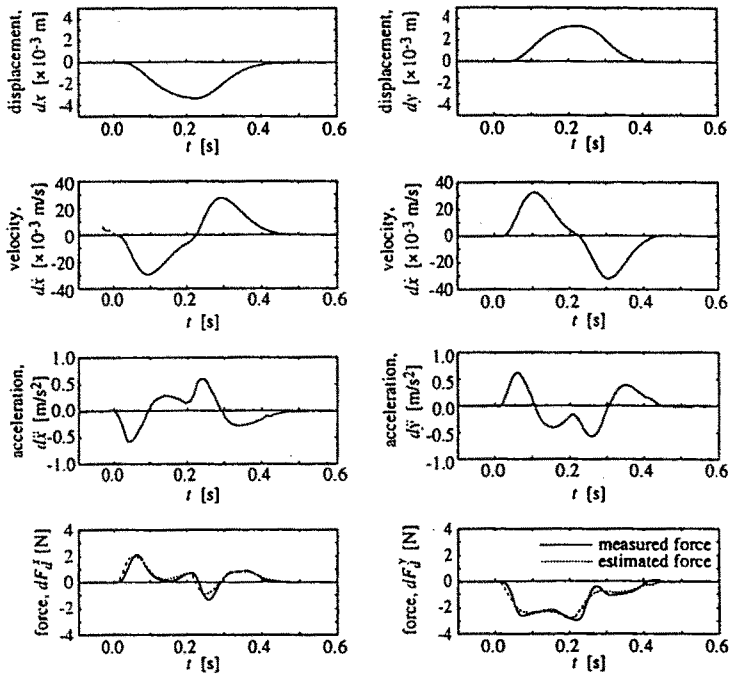

Figure 6: Example of measured human hand motion and force in experiment 2), where the target activation level was 10 percent of the MVC

4.2 Elliptical plot of the estimated hand impedance

The impedance ellipses corresponding to the symmetrical components of the mean values of the estimated impedance matrices for ten data sets of experiment 1) are shown in Fig. 7 (Tsuji et al. 1994). Figure 7 (a) shows inertia ellipses that graphically represent the locus of the hand force vectors determined by an input disturbance consisting of an acceleration vector of unit length (1 m/s^2) rotated in all possible directions (Mussa-Ivaldi et al. 1985, Hogan 1985).

The inertia matrices from the motion equation of the two-link arm model are also computed using (17), which are based on anatomical measurements of the link lengths of each subject and estimated values

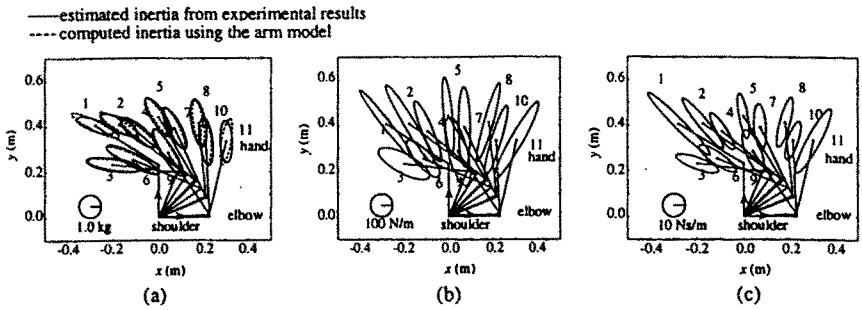

Figure 7: Estimated impedance ellipses. (a) Inertia, (b) stiffness and (c) viscosity

of the corresponding masses and moments of inertia using the method of Winter (1979). The dashed ellipses in Fig. 7 (a) show the computed results. It can be seen that in qualitative terms, the human hand inertia characteristics in multi-joint movements can be explained from basic biomechanics.

Figure 7 (b) and (c) show stiffness and viscosity ellipses corresponding to the inertia ellipses in Fig. 7 (a). The major axis of the viscosity ellipse is nearly coaligned with the corresponding stiffness ellipse, and that the shapes of the viscosity ellipses become thinner near the distal boundary of the work space in the almost same manner as the stiffness ellipses (Tsuji et al. 1995).

Next, a change of the impedance ellipses of a subject with the target muscle activation level estimated from the results of experiment 2) is shown in Fig. 8 (Tsuji & Kaneko 1996). The solid, dashed, and alternate long and short dashed ellipses represent the mean values of ten data sets of the experimental results corresponding to the target muscle activation levels of 0, 10, 20 percents of the MVC, respectively, and the dotted ellipse represents the hand inertia computed from the motion equation of the two-link arm model. It can be seen from the figure that the stiffness and viscosity ellipses change largely with the target muscle activation level, while a large variation is not observed for the inertia ellipse.

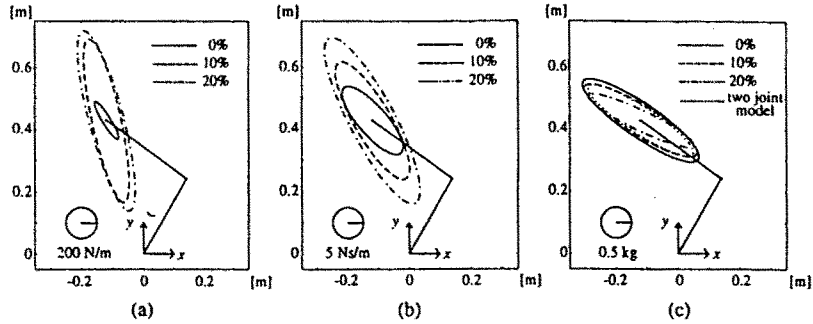

Figure 8: Changes of hand impedance ellipses with target muscle contraction levels (subject C). (a) Stiffness, (b) viscosity and (c) inertia

The hand stiffness ellipses computed using the mean values of ten data sets estimated in experiment 3) are represented in Fig. 9 (Tsuji & Kaneko 1996), which are arranged according to the eight different directions of the target hand force in each figure (see Fig. 5). The stiffness ellipses show that the area, orientation and shape of the ellipses change depending on the target hand force even if the arm posture does not change. It should be noted that the characteristics of the hand impedance were also observed similarly for other subjects.

5 Modeling human arm impedance

5.1 Muscle impedance model

Using the kinematic relationships among the muscle, joint and endpoint levels, the transformations of the stiffness and viscosity matrices can be written as (10)–(13). The Jacobian matrix J can be determined by the arm kinematics, so that the joint viscoelastic matrices can be computed from the corresponding hand impedance estimated experimentally. In this section, the relationship between the joint and muscle stiffness are analyzed based on (11). It should be noted that the viscosity analysis will be also held in the same manner.

The Jacobian matrix G and the muscle stiffness matrix K_m included

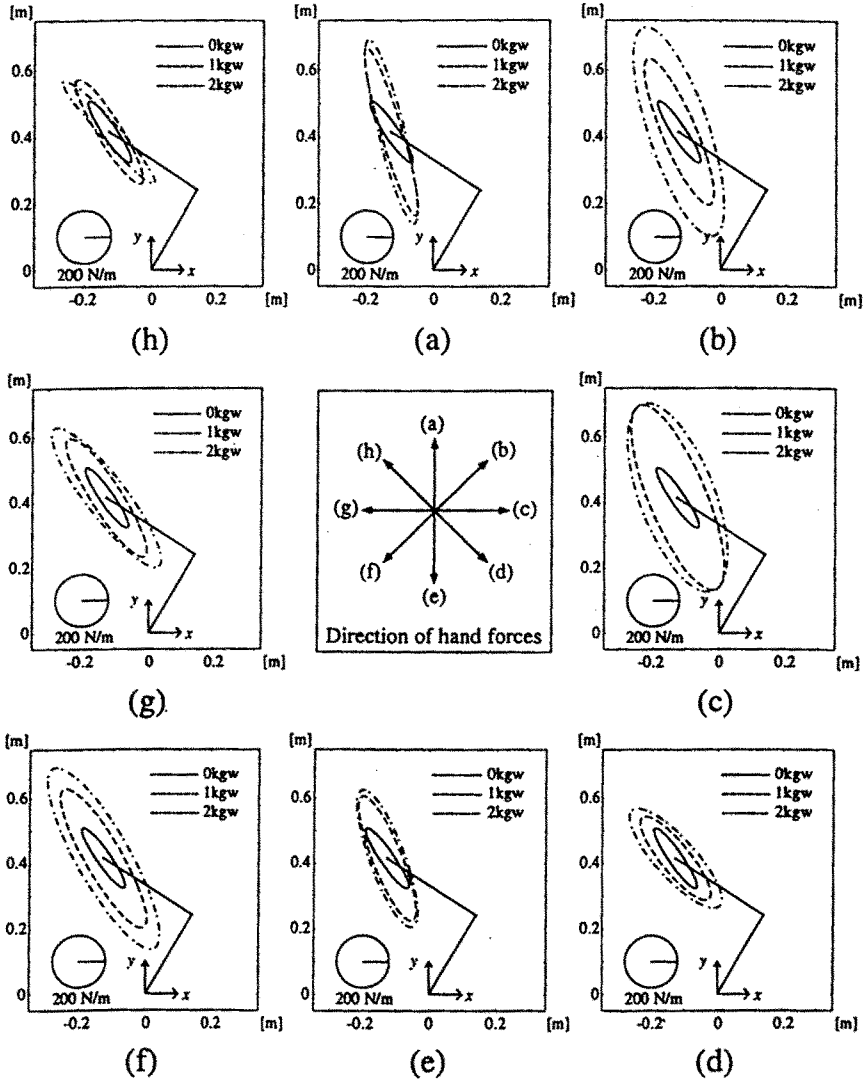

Figure 9: Changes of hand stiffness ellipses with direction and amplitude of the target hand forces (subject C)

in (11) are represented as follows:

$$G = \begin{pmatrix} -d_{1s}(\theta) & d_{2s}(\theta) & 0 & 0 & -d_{5s}(\theta) & d_{6s}(\theta) \\ 0 & 0 & -d_{3e}(\theta) & d_{4e}(\theta) & -d_{5e}(\theta) & d_{6e}(\theta) \end{pmatrix}^T, \quad (30)$$

$$K_m = diag.[f_1(\alpha_1),\ f_2(\alpha_2),\ \cdots,\ f_6(\alpha_6)], \quad (31)$$

where $d_{ij}(\theta) > 0 (i = 1, 2, \cdots, 6; j = s, e)$ is the length of the moment arm of muscle i to the shoulder (s) or elbow (e) joint; $f_i(\alpha_i) > 0$ is the stiffness of the muscle i; and diag. [ ] denotes the diagonal matrix. Also $\theta = (\theta_s, \theta_e)^T$ denotes the joint angle vector. Each low and column of the matrix G corresponds to each joint and muscle, respectively. The single-joint muscle has no effect to the other joint, so that the corresponding elements in (30) becomes 0. Also, the Jacobian matrix J for the two-joint arm is given as

$$J = \begin{pmatrix} -l_1 \sin\theta_s - l_2 \sin(\theta_s + \theta_e) & -l_2 \sin(\theta_s + \theta_e) \\ l_1 \cos\theta_s + l_2 \cos(\theta_s + \theta_e) & l_2 \cos(\theta_s + \theta_e) \end{pmatrix}, \quad (32)$$

where l_1 and l_2 are the length of the forearm and the upper arm, respectively. Substituting (30)–(32) into (11), each element of the joint stiffness matrix can be represented as

$$K_{ss} = d_{1s}^2(\theta) f_1(\alpha_1) + d_{2s}^2(\theta) f_2(\alpha_2) + d_{5s}^2(\theta) f_5(\alpha_5) + d_{6s}^2(\theta) f_6(\alpha_6), \quad (33)$$

$$K_{se} = d_{5s}(\theta) d_{5e}(\theta) f_5(\alpha_5) + d_{6s}(\theta) d_{6e}(\theta) f_6(\alpha_6), \quad (34)$$

$$K_{ee} = d_{3e}^2(\theta) f_3(\alpha_3) + d_{4e}^2(\theta) f_4(\alpha_4) + d_{5e}^2(\theta) f_5(\alpha_5) + d_{6e}^2(\theta) f_6(\alpha_6). \quad (35)$$

In experiment 1), the arm posture of the subject were changed depending on the different hand location, while the muscle activation levels during measurements were almost constant. Therefore we can concentrate on the postural effects to the arm impedance under the assumption of the constant muscle activity. On the other hand, in experiments 2) and 3), the muscle activation levels were varied widely under the constant arm posture, so that the muscular effects to the arm impedance appears clearly.

Table 1: Accuracy of fitting results of joint impedance for subject A. R and E in the table denote the correlation coefficients between the measured and predicted joint impedance and the squared sum of the prediction errors, respectively

			K_{ss}	K_{se}	K_{es}	K_{ee}	B_{ss}	B_{se}	B_{es}	B_{ee}
Subject A	$L=0$	R	0.000	0.000	0.000	0.000	0.000	0.000	0.000	0.000
		E	109.205	27.796	26.657	50.011	1.013	0.181	0.193	0.263
	$L=1$	R	0.778	0.732	0.740	0.776	0.785	0.742	0.806	0.486
		E	43.077	16.329	15.551	19.915	0.389	0.090	0.077	0.201
	$L=2$	R	0.978	0.915	0.890	0.976	0.967	0.947	0.962	0.916
		E	4.848	9.877	10.560	2.345	0.064	0.032	0.028	0.042

5.2 Postural effects

The length of the moment arm of muscle i is approximated by an L-th order polynomial of the corresponding joint angle:

$$d_{ij}(\theta) = \sum_{k=0}^{L} a_{ijk}\theta_j^k \tag{36}$$

for single-joint muscles, $i = 1,2,3,4$ and $j = s,e$, and

$$d_{ij}(\theta) = \sum_{k=0}^{L}\sum_{l=0}^{k} b_{ijkl}\theta_s^l\theta_e^{k-l} \tag{37}$$

for two-joint muscles, $i = 5,6$ and $j = s,e$. Substituting (36), (37) into (33)–(35) yields a set of the $2L$-th order polynomials for each element of the joint stiffness, since the muscle activation level, α_i, can be considered as a constant for each muscle in experiment 1).

Using the mean values of the joint stiffness for ten data sets estimated in experiment 1), coefficients included in the polynomials were estimated by the standard least square method. Table 1 shows the estimated results for subject A, in which the correlation coefficients between the measured and predicted joint stiffness and the squared sum of the prediction errors are shown. Both the correlation coefficients and the prediction errors improve, as the order of the polynomial L

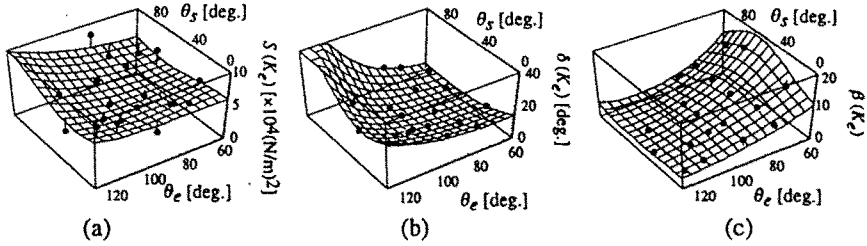

Figure 10: Changes of geometrical parameters of the hand stiffness ellipses with the shoulder and elbow joint angles (subject A). (a) Size, (b) orientation and (c) shape

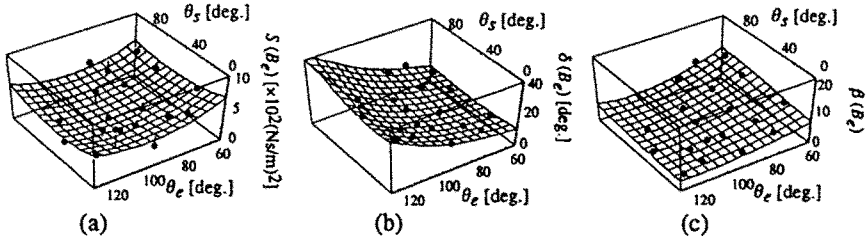

Figure 11: Changes of geometrical parameters of the hand viscosity ellipses with the shoulder and elbow joint angles (subject A). (a) Size, (b) orientation and (c) shape

increases. In the table, the estimated results for the joint viscosity are also shown. It can be seen that the joint viscoelasticity can be approximated by using the polynomial model of the length of the muscle moment arm with the appropriate order (more than $L = 1$).

Figures 10 and 11 show the changes of the three parameters of the hand stiffness and viscosity ellipses, that is, (1) the size defined by the area of the ellipse, (2) the orientation defined by the counter-clockwise angle from the line passing the positions of the shoulder joint and the hand to the major axis of the ellipse, and (3) the shape defined by the ratio between the lengths of the minor axis and the major axis (Flash & Mussa-Ivaldi 1990, Dolan et al. 1993). The parameters defined above represent the magnitude, the direction and the directional change of the

hand stiffness and viscosity, respectively. In the figure, the predicted values of the parameters using the first order polynomial models are represented as the 3D surfaces and the measured values are shown as the black circles simultaneously. It can be seen that the hand stiffness and viscosity of the subject can be predicted with a sufficient accuracy.

5.3 Muscular effects

Then the stiffness and viscosity of the muscle i is approximated by an N-th order polynomial of the corresponding muscle activation level, α_i:

$$f_i(\alpha_i) = \sum_{k=0}^{N} c_{ik}\alpha_i^k \tag{38}$$

for all muscles, $i = 1, 2, \cdots, 6$. Substituting (38) into (33)–(35) yields a set of the N-th order polynomials for each element of the joint stiffness, since the moment arm of each muscle, $d_{ij}(\theta)$, can be considered to be constant in experiments 2) and 3).

Using the joint stiffness for ten data sets estimated in experiments 2) and 3), which consist of five data sets measured in one day for each experiment, coefficients included in the polynomials were estimated by the standard least square method. Tables 2 shows the estimated results for subject B with the ones for the joint viscosity. The joint viscoelasticity can be approximated by using the polynomial model

Table 2: Accuracy of fitting results of joint impedance for subject B. The N-th order polynomial model for the muscle viscoelasticity is used

			K_{ss}	K_{se}	K_{ee}	B_{ss}	B_{se}	B_{ee}
Subject B	$N=1$	R	0.595	0.645	0.917	0.796	0.609	0.891
		E	7218.09	4194.83	3056.50	15.58	7.94	5.59
	$N=2$	R	0.739	0.649	0.944	0.855	0.616	0.914
		E	5064.28	4157.62	2077.05	11.43	7.83	4.47
	$N=3$	R	0.841	0.661	0.948	0.874	0.629	0.918
		E	3261.07	4042.04	1931.65	10.06	7.64	4.25

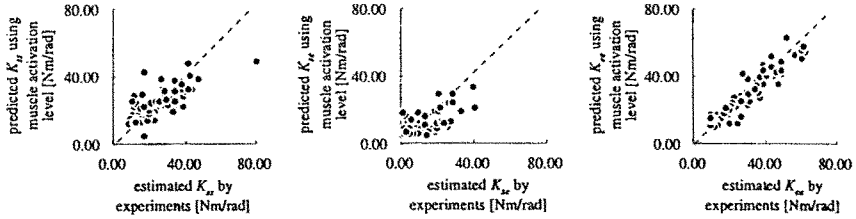

Figure 12: Predicted joint stiffness by using the second order polynomial model for the muscle stiffness with measured muscle activation level (subject B)

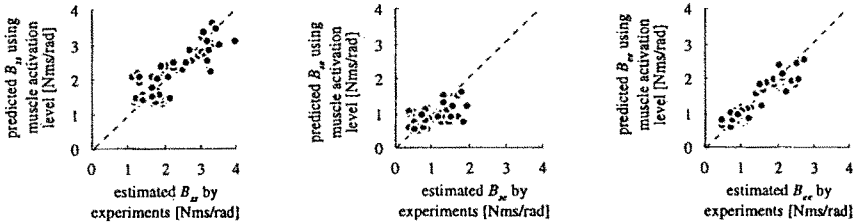

Figure 13: Predicted joint viscosity by using the second order polynomial model for the muscle viscosity with measured muscle activation level (subject B)

of the muscle viscoelasticity with the appropriate order (more than $N = 2$) under the constant posture.

Figures 12 and 13 show the accuracy of the predicted joint stiffness and viscosity for the experimental results of subject B, where the vertical axis represents the joint stiffness and viscosity computed from the experimental results and the horizontal axis represents the ones predicted by using the second order polynomial model of the muscle viscoelasticity. The joint stiffness computed from the experimental results agrees well with the predicted values.

Figure 14 shows the predicted changes of the hand stiffness ellipses with the activation levels of the single-joint muscles, where the activation levels of the flexors and the extensors are set to be $\alpha_1 = \alpha_3$ and $\alpha_2 = \alpha_4$, and the activation levels of the two -joint muscles used in the

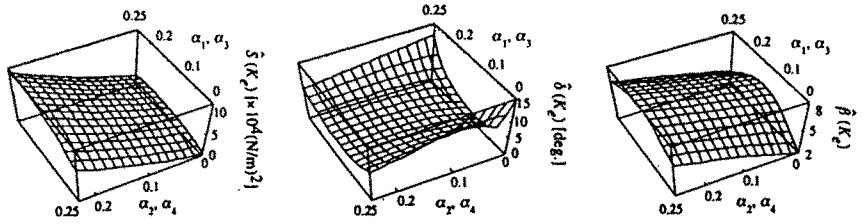

Figure 14: Predicted changes of geometrical parameters of the hand stiffness ellipses with the activation levels of the single-joint muscles. (a) Size, (b) orientation and (c) shape

figure are $\alpha_5 = \alpha_6 = 0.1$. In the figure, the predicted changes of three parameters of the hand stiffness are shown as the 3D surfaces. The measurements of the EMG signals and the joint angles are much easier than the estimation procedure of the hand impedance and can be performed without preventing movements of the subject. Therefore, the prediction of the hand impedance described here may be a very useful technique for some purposes such as the control of the human-robot interactions and the analysis of skillful human movements in sports.

6 Conclusion

The purpose of this chapter was to investigate the spatial characteristics of the hand impedance in multi-joint movements during isometric muscle contraction and to make clear the dependency on the arm posture and muscle activity. The main results of the experiments can be summarized as follows: (1) the human hand inertia characteristics can be explained from basic biomechanics of the passive inertial effects, (2) the spatial variations of the estimated hand stiffness ellipses depending on the arm posture approximately agreed with the experimental results of other researchers (Mussa-Ivaldi et al. 1985, Flash & Mussa-Ivaldi 1990, Dolan et al. 1993) except for the size of the ellipses, (3) the co-contraction of the flexor and the extensor increases the sizes of the hand stiffness and viscosity ellipses, (4) the geometrical param-

eters of the hand stiffness and viscosity ellipses while generating the constant hand force change depending on the amplitude and direction of the hand force, and (5) the hand stiffness and viscosity can be predicted with a sufficient accuracy under the assumptions that the length of the muscle moment arm and the muscle viscoelasticity can be approximated by polynomial models of the joint angles and the muscle activation levels estimated from the EMG signals, respectively.

The estimated impedance including stiffness, viscosity and inertia of human arm can provide a basic data for simulation studies of the multi-joint movements, such as computer simulations of two-joint arms by Flash (1987) based on the virtual trajectory control hypothesis and Katayama & Kawato (1993) based on internal models of motor control systems which are acquired through biological motor learning. Also, the arm impedance model derived here may be useful for the control of human-robot interactions in which the impedance characteristics of human arm are often used as a model of a human operator.

However, in this chapter, only the arm impedance in the stationary state of the muscle activation level and hand force have been analyzed. Future research will be directed to make clear how the arm impedance changes in the transient states of the muscle activation levels and to apply the arm impedance characteristics of human arm derived here to the control of human-robot interactions.

Acknowledgments

The author would like to thank to Prof. Pietro G. Morasso, Prof. Koji Ito, Prof. Makoto Kaneko, and Dr. Mikhail Svinin for their helpful comments and discussions. The author is also favored to have the assistance of Kazuhiro Goto, Masamitsu Moritani and Tomoaki Shibata who contributed their experimental skill and sustained efforts.

References

Asada, H. & Slotine, J. (1986). *Robot analysis and Control*, John Wiley.

Bennett, D. J., Hollerbach, J. M., Xu, Y. & Hunter, I. W. (1992). Time varying stiffness of human elbow joint during cyclic voluntary movement, *Experimental Brain Research* **88**: 433–442.

Cannon, S. & Zahalak, G. I. (1982). The mechanical behavior of active human skeletal muscles in small oscillations, *Journal of Biomechanics* **15**: 111–121.

Dolan, J. M., Friedman, M. B. & Nagurka, L. (1993). Dynamic and loaded impedance components in the maintenance of human arm posture, *IEEE Transaction on System, Man, and Cybernetics* **23**(3): 698–709.

Dowben, R. M. (1980). Contractility, *in* V. B. Mountcastle & C. V. Mosby (eds), *Medical Physiology 14th.*, pp. 82–119.

Flash, T. (1987). The control of hand equilibrium trajectories in multi-joint arm movement, *Biological Cybernetics* **57**: 257–274.

Flash, T. & Mussa-Ivaldi, F. A. (1990). Human arm stiffness characteristics during maintenance of posture, *Experimental Brain Research* **82**: 315–326.

Gomi, H. & Kawato, M. (1996). Equilibrium-point control hypothesis examined by measured arm stiffness during multijoint movement, *Science* **272**: 117–120.

Gomi, H., Koike, Y. & Kawato, M. (1992). Human hand stiffness during discrete point-to-point multi-joint movement, *Proceedings of the Annual International Conference of the IEEE Engineering in Medicine and Biology Society*, pp. 1628–1629.

Hogan, N. (1985). The mechanics of multi-joint posture and movement control, *Biological Cybernetics* **53**: 1–17.

Katayama, M. & Kawato, M. (1993). Virtual trajectory and stiffness ellipse during multi-joint arm movement predicted by neural inverse models, *Biological Cybernetics* **69**: 353–362.

Khatib, O. (1987). A unified approach for motion and force control of robot manipulators: operational space formulation, *IEEE Journal of Robotics and Automation* **RA–3**(1, Feburuary).

Lacquaniti, F., Licata, F. & Soechting, J. F. (1982). The mechanical behavior of the human forearm in response to transient perturbations, *Biological Cybernetics* **44**: 35–46.

MacKay, W. A., Crammond, D. J., Kwan, H. C. & Murphy, J. T. (1986). Measurements of human forearm viscoelasticity, *Journal of Biomechanics* **19**: 231–238.

Milner, T. E. (1993). Dependence of elbow viscoelastic behavior on speed and loading in voluntary movements, *Experimental Brain Research* **93**: 177–180.

Mussa-Ivaldi, F. A. (1986). Compliance, *in* P. Morasso & V. Tagliasco (eds), *Human Movement Understanding*, Elsevier, pp. 161–212.

Mussa-Ivaldi, F. A., Hogan, N. & Bizzi, E. (1985). Neural, mechanical and geometrical factors subserving arm posture in humans, *Journal of Neuroscience* **5**(10): 2732–2743.

Tsuji, T., Goto, K., Moritani, M., Kaneko, M. & Morasso, P. (1994). Spatial characteristics of human hand impedance in multi-joint arm movements, *Proceedings of IEEE International Conference on Intelligent Robots and Systems*, pp. 423–430.

Tsuji, T. & Kaneko, M. (1996). Estimation and modeling of human hand impedance during isometric muscle contraction, *Proceedings of the Fifth Annual Symposium on Haptic Interface for Virtual Environment and Teleoperator Systems*. in press.

Tsuji, T., Morasso, P., Goto, K. & Ito, K. (1995). Human hand impedance characteristics during maintained posture, *Biological Cybernetics* **72**: 475–485.

Winter, D. A. (1979). *Biomechanics of human movement*, A Willy-Interscience Publication.